Spin-Transistor Action via Tunable Landau-Zener Transitions

C. Betthausen *et al.*

Science **337**, 324 (2012);
DOI: 10.1126/science.1221350

Science (print ISSN 0036-8075; online ISSN 1095-9203) is published weekly, except the last week in December, by the American Association for the Advancement of Science, 1200 New York Avenue NW, Washington, DC 20005.

Spin-Transistor Action via Tunable Landau-Zener Transitions

C. Betthausen,[1] T. Dollinger,[2] H. Saarikoski,[2] V. Kolkovsky,[3] G. Karczewski,[3] T. Wojtowicz,[3] K. Richter,[2] D. Weiss[1]*

Spin-transistor designs relying on spin-orbit interaction suffer from low signal levels resulting from low spin-injection efficiency and fast spin decay. Here, we present an alternative approach in which spin information is protected by propagating this information adiabatically. We demonstrate the validity of our approach in a cadmium manganese telluride diluted magnetic semiconductor quantum well structure in which efficient spin transport is observed over device distances of 50 micrometers. The device is turned "off" by introducing diabatic Landau-Zener transitions that lead to a backscattering of spins, which are controlled by a combination of a helical and a homogeneous magnetic field. In contrast to other spin-transistor designs, we find that our concept is tolerant against disorder.

The use of electron spin to store and process information calls for the ability to inject, propagate, and manipulate spin with high efficiency (*1*, *2*). Much of the recent research in the field has been motivated by attempts to realize the seminal spin transistor proposed by Datta and Das (*3*). Their original concept requires spin injection from ferromagnetic contacts into a narrow channel of a two-dimensional electron gas (2DEG), where transport is ballistic and spins precess in a gate-controlled spin-orbit field into "on" or "off" orientations. Even though such spin manipulation in a spin-orbit field has been demonstrated in a nonlocal measurement (*4*), signal levels remain small as a result of low spin-injection efficiency and limited spin lifetime. The latter can be enhanced if spin polarization is protected against scattering processes by an SU(2) symmetry that emerges when the Rashba spin-orbit interaction strength is equal to the Dresselhaus term (*5*, *6*). This creates a persistent spin-helix state (*6*) that has been observed in optical measurements (*7*). Aside from 2D systems, spin-transistor action was also explored in bulk bipolar semiconductors (*8*, *9*).

Here, we present an alternative efficient spin-transistor design that uses adiabatic spin propagation to protect spin information and tunable diabatic Landau-Zener transitions between spin eigenstates for spin-transmission control (Fig. 1). According to the adiabatic theorem of quantum mechanics (*10*), a spin that is initially in an eigenstate will remain in its instantaneous eigenstate during transport if external perturbations act on it slowly. Spin information is hence protected against decay, allowing spin to propagate over device distances of several micrometers. For rapidly changing perturbations, spin cannot adapt its state, which becomes a superposition of eigenstates. This causes diabatic Landau-Zener transitions between the spin eigenstates (*11*, *12*), which can be used to selectively backscatter spin-polarized charge carriers, thus giving rise to transistor action.

We demonstrate the validity of our approach in a (Cd,Mn)Te diluted magnetic semiconductor quantum-well (QW) structure in which the giant Zeeman splitting, attributed to *s-d* exchange interaction between electronic states and the localized Mn spins (*13*), gives rise to intrinsic spin polarization. We modulate the diabatic spin-backscattering probability by a combination of a spatially rotating magnetic field $\mathbf{B}_s$ and a homogenous magnetic field $\mathbf{B}$. $\mathbf{B}_s$ is created by premagnetized ferromagnetic stripes placed above the device (Fig. 2, A and D). In the absence of the homogeneous field, eigenfunctions change slowly, leading to adiabatic spin transport and a helical spin wave resulting from U(1) symmetry. If scattering is spin-independent, spin orientation depends only on the position along the transport direction and not on the specific path of the spin: the device is in its on state. However, if the helical field component is equal in amplitude to the homogeneous component, diabatic transitions and backscattering of spin occur. Consequently, the device is in the off state. As in the original Datta-Das concept, we measure the source-drain resistance, which intensifies as the spin-backscattering rate is increased. The degree of adiabaticity is therefore monitored electrically in the channel resistance, in contrast to interference measurements (*14*, *15*) of geometrical (Berry) phases (*16*), associated with adiabatic spin evolution only.

Our setup consists of three building blocks: (i) a high-mobility 2DEG with a giant Zeeman splitting, (ii) a grating of ferromagnetic stripes on top of the sample (Fig. 2, A and D), and (iii) a homogeneous B field generated by a superconducting coil. A modulation doped (Cd,Mn)Te quantum-well structure (*17*, *18*) is used to confine electrons to two dimensions. The ferromagnetic grating is made of 75-nm-thick dysprosium stripes patterned to periods a ranging from 0.5 to 8 μm. The stripes are premagnetized in a field of 8 T, which gives rise to a remnant magnetization of 0.7×10^6 A/m, determined by superconducting quantum interference device (SQUID) measurements. In the plane of the 2DEG, the stray field of the periodic grating of magnets is approximately helical with an amplitude of ~50 mT (Fig. 2B). The magnetic field texture translates to a helical spin polarization via the giant Zeeman coupling. In our devices, we use the beating pattern of the Shubnikov–de Haas oscillations at low fields (Fig. 2E) to estimate a Zeeman splitting of 1 meV for a 50-mT stray field at 25 mK (*18*, *19*). The Zeeman energy E_Z is the largest spin-dependent energy scale; Rashba and Dresselhaus spin-orbit splittings are more than one order of magnitude smaller (*20*). Spin polarization $p = (n_\downarrow - n_\uparrow)/(n_\uparrow + n_\downarrow) \approx E_Z/2E_F$ in the 2DEG ranges from 8 to 15% in a 50-mT stray field for our samples (Fig. 2, C and D). Here, $n_{\uparrow,\downarrow}$ denotes the density of spin-up/down electrons; E_F is the Fermi energy.

To measure the longitudinal resistance $\rho_{xx}(B)$ in a Hall bar geometry, the magnetic field is first ramped up to 8 T under an angle θ (Fig. 2A) to magnetize the stripes, and then data are taken on the sweep back to –0.5 T. In the presence of a helical stray field, $\rho_{xx}(B)$ shows distinct peaks at about ±50 mT (Fig. 2, E and F) for the studied devices A, B, and C (fig. S1). The samples differ in QW thickness, carrier density, electron mobility, and Mn concentration (table S1), but the results are independent of such details. The peaks do not appear in unmodulated reference samples. Apart from a small dip near $B = 0$, reminiscent of weak antilocalization (black traces in Fig. 2F), these samples do not show any notable

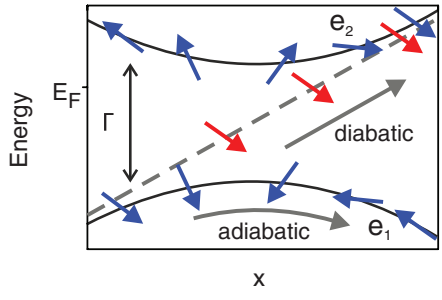

Fig. 1. Spin-transistor action via tunable diabatic transitions in a system of two orthogonal spin-eigenstates e_1 and e_2 (blue arrows) with energy separation Γ at the closest approach. A spin that is transported along a spatial coordinate x through the system, starting from e_1, will remain in this instantaneous eigenstate if evolution (here defined as rotation of eigenstate spin orientation) is slow in the reference frame of the spin (small dx/dt). In a fast evolution (large dx/dt), spin cannot adapt to the changing environment, leading to a diabatic evolution (red arrows) corresponding to a Landau-Zener transition to e_2. The e_2 state lies above E_F, causing wave-function decay and spin backscattering. Spin-transistor action involves either tuning Γ or dx/dt.

[1]Department of Experimental and Applied Physics, Regensburg University, 93040 Regensburg, Germany. [2]Department of Theoretical Physics, Regensburg University, 93040 Regensburg, Germany. [3]Institute of Physics, Polish Academy of Sciences, 02668 Warsaw, Poland.

*To whom correspondence should be addressed. E-mail: dieter.weiss@physik.uni-regensburg.de

features at low B. The ρ_{xx} peaks in the modulated samples vanish rapidly with increasing temperature T and are no longer recognizable above ~0.6 K (Fig. 3A). This behavior, confirmed by full numerical transport calculations in Fig. 3B (*18*), is expected for the spin polarization of (Cd,Mn)Te, as the dominant *s-d* exchange part in the g factor contributes appreciably only at low T. Because of their orbital nature, magnetic commensurability effects persist to much higher T (~40 K) (*21*) and can therefore be excluded. Hence, the T dependence of the peaks confirms a spin-related effect.

The ρ_{xx} peaks reflect reduced spin transmission through the 2DEG channel, which can be intuitively explained within the following model: Due to the high mobility of our samples, let us assume that the spin transport is ballistic on the scale of the period of the Dy grating. Figure 2C shows the Zeeman-split subbands of a 2DEG. At E_F there is an imbalance of spin states moving in the x direction because some of the occupied spin-split modes exhibit unoccupied counterparts above E_F. For a Zeeman-split state pair close to E_F, the upper state (solid blue line in Fig. 2C) is unoccupied, whereas the lower state (solid red line) is occupied and carries spin. Assuming a helical stray field (*22*, *23*) with amplitude B_s, the total magnetic field, $\mathbf{B} + \mathbf{B_s(x)}$, gives rise to a Zeeman splitting $E_{Z,\pm(x)} = \pm\frac{1}{2} g_{\mathrm{eff}} \mu_B B_s \sqrt{1 + \gamma^2 + 2\gamma\cos(2\pi x/a)}$, where $\gamma = B/B_s$, g_{eff} is the (giant) effective g factor of (Cd,Mn)Te, and μ_B is Bohr's magneton.

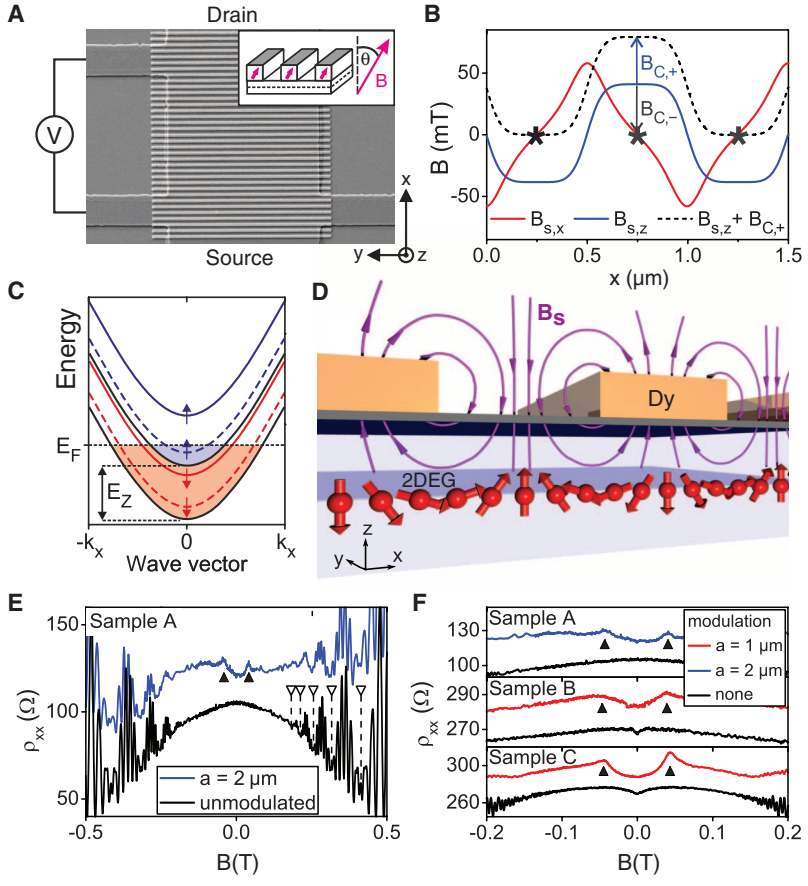

Fig. 2. (**A**) Electron micrograph of a Hall-bar segment covered with Dy stripes. (Inset) Orientations of the external homogeneous B field and the magnetic moments of the premagnetized stripes (magenta arrows), defined by the tilt angle θ with respect to the z axis in the xz plane. (**B**) Calculated magnetic stray-field components $B_{s,x}$ (red) and $B_{s,z}$ (blue) in the plane of the 2DEG for sample C with a grating of a = 1 μm. $B = B_{C,+}$ and $B = B_{C,-}$ denote the external field needed to generate points of vanishing total magnetic field (marked by asterisks) if the external field is applied in positive or negative z direction, respectively. (**C**) Schematic band structure of the (Cd,Mn)Te QW. Black solid lines, Zeeman-split spin-up and spin-down subbands for wave vectors in the y direction, $k_y = 0$; dashed lines, spin-split subbands for $k_y \neq 0$, but with spin-up and spin-down states occupied at E_F; colored solid lines, spin-split subbands for $k_y \neq 0$, but with an empty upper band. Only Landau-Zener transitions between filled and empty subbands contribute to spin backscattering. Spin-up and spin-down densities $n_\uparrow$ and $n_\downarrow$ are represented by blue and red areas, respectively. (**D**) In the adiabatic transport regime at $B = 0$, electron spins in the 2DEG (spheres with arrows) keep anti-aligned with the stray-field B_s of the stripes, and a spin-helix forms. (**E** and **F**) ρ_{xx} with and without modulation at T = 25 mK and θ = 0° (upper curves, shifted for clarity). Mn ions in the QW cause a distinct beating pattern with nodes (open triangles) at higher B (E). Resistance peaks (black triangles) are associated with blocking of spin transmission.

For one pair of spin-polarized states (that is, for fixed wave vector k_y), the total magnetic field, Zeeman-split energy levels, spin directions, and local energy bands are depicted in Fig. 3E (case $B = B_s/2$) and Fig. 3F ($B = B_s$). Because of the large Zeeman splitting associated with the stray field at $B = 0$, the Larmor frequency $\omega_L = g_{\mathrm{eff}}\mu_B B_s/\hbar$ (where $\hbar$ is Planck's constant h divided by 2π) is higher than the frequency of stripe modulation in a ballistic flight through the device $\omega_f = 2\pi v_{F,x}/a$ (where $v_{F,x} = \hbar k_x/m^*$ is the component of the Fermi velocity parallel to the transport direction, m^* is the effective mass of CdTe, and k_x is the wave vector in x direction). This keeps spin transport predominantly in the adiabatic regime, as expressed by the condition $Q = \omega_L/\omega_f > 1$, where Q is a measure of the degree of adiabaticity in ballistic systems (*16*, *24*, *25*). For $B = B_s$, a degeneracy point emerges in the energy bands midway between adjacent stripes, because the total magnetic field vanishes at those points (Figs. 2B and 3F). In the reference frame of the spin, the direction of the magnetic field first rotates continuously as it approaches the degeneracy point adiabatically, but then the field reverses direction. This violates the conditions for adiabaticity, because an instant 180° spin-rotation would be needed to stay on the lower band. Hence, a transition to the upper Zeeman band occurs close to the degeneracy. On the upper band the spin is parallel to the magnetic field, giving rise to a tunneling barrier because the potential energy rises above E_F; this leads to backscattering, and spin-transport is blocked, increasing the resistance of the sample. Only spin-polarized modes are affected by this blocking, because both spin bands of spin-compensated modes remain everywhere below E_F.

The probability of a diabatic transition to the upper Zeeman band is finite, even if there are no degeneracy points. Using Landau-Zener formalism, we show (*18*) that the spin-backscattering probability associated with a diabatic transition becomes increasingly probable as the distance between the Zeeman-split levels at the closest approach decreases or transport velocity $v_{F,x}$ increases (*11*, *12*, *26*). The periodic stripe grating forms a spatially repeating sequence of potential transition points that enhances the probability of a diabatic transition.

The actual stray-field profile of the magnetized stripes is anisotropic and only approximately helical (Fig. 2B). This provides an additional means to confirm that the ρ_{xx} peaks stem from spin-transmission blocking. To do that, we studied samples with different stripe periodicities a ranging from 0.5 to 8 μm (shown for θ = 45° in Fig. 3C) and measured $\rho_{xx}(B)$ at different tilt angles θ for a given value of a (shown for a = 1 μm in Fig. 3D). We calculated the stray field of the stripes within the dipole approximation for different values of θ and a, which gives the positions of the spin-blocking peaks as field values where zeros form in the total field. Our theoretical data are compared with the corresponding values

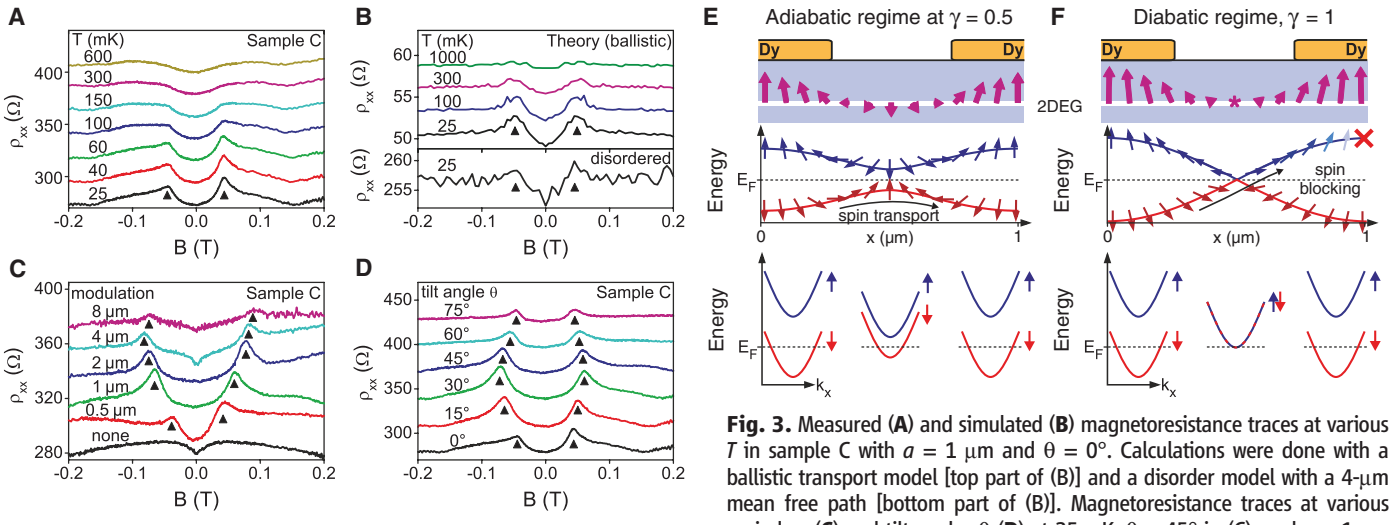

Fig. 3. Measured (**A**) and simulated (**B**) magnetoresistance traces at various T in sample C with a = 1 μm and θ = 0°. Calculations were done with a ballistic transport model [top part of (B)] and a disorder model with a 4-μm mean free path [bottom part of (B)]. Magnetoresistance traces at various periods a (**C**) and tilt angles θ (**D**) at 25 mK, θ = 45° in (C), and a = 1 μm in (D). All curves, except the lowest ones, in (A) to (D) are shifted for clarity. (**E** and **F**) Total magnetic field acting on an electron (top panels) and Zeeman-split energy-bands of a polarized state (middle panels) with spin-orientations (arrows) in the (E) adiabatic transport regime at $\gamma = B/B_s = {}^1/_2$ and in the (F) diabatic regime $\gamma = 1$. The x component of magnetic field reverses direction in the center at $\gamma = 1$, which leads to spin backscattering. (Bottom panels) Corresponding local Zeeman-split energy bands.

extracted for sample C in Fig. 4A (and for sample B in fig. S3) and show the expected anisotropy. Note that no fit parameters were used in the calculations.

In the ballistic model, all spin-polarized transport modes are blocked at $B = B_s$, increasing the resistance of the sample. A single degeneracy point in the Zeeman bands is sufficient to block all spin transmission; hence, the peak height does not depend on the number of modulations, which is in line with the measurements of different modulation periods at a fixed device length of 50 μm (Fig. 3C). Only the 8-μm modulation shows a reduced peak height, which is probably due to the highly anisotropic stray field.

The ballistic model gives an estimate $E_Z(T,2B_s)/(4E_F)$ for the relative magnetoresistance peak height $\Delta\rho_{xx}/\rho_{xx}$ (black line in Fig. 4B). In the presence of disorder, diabatic transitions are perturbed and, hence, peak heights are reduced. However, we found that disorder does not strongly affect the measured peak heights in sample C. The experimental values in Fig. 4B are comparable to our disorder model at an electron mean free path of l_e = 4 μm (blue triangles in Fig. 4B). The peaks disappear in the calculations at l_e = 0.65 μm, which equals the measured mean free path in sample C. Orbital effects may enhance spin effects and contribute to a better-than-expected device performance at low T (*18*). Nevertheless, experiments indicate that adiabatically transported spin is stable over device distances of 50 μm, which are much longer than electron mean free paths in the samples (between 0.47 and 1.39 μm).

Our results demonstrate the concept of an adiabatic spin transistor: Adiabatic transport protects spin information, whereas diabatic transitions lead to spin backscattering (thus depolarizing the current) and allow for switching between on and off states. In contrast to the Datta-Das concept, our approach is tolerant against disorder. Our proof of concept device shows source-drain resistance modulation of up to ~10%, which is expected to be considerably enhanced in materials with high spin polarization (*18*). Furthermore, the homogeneous B field, provided here by coils, might be replaced with a magnetic gate that is switched by spin torque, discussed in (*18*). This would enable the device to be controlled purely by electric fields. As we use a paramagnetic material, our device operates only at low T. However, we stress that the design concepts are not restricted to a particular choice of materials, temperature, methods of spin injection, manipulation, or detection. Transferring our concept to higher T requires employing exchange or spin-orbit splitting rather than Zeeman splitting. Possible material systems in which exchange interaction can be tuned by means of an electric field involve, for instance, magnetic semiconductors (*27*).

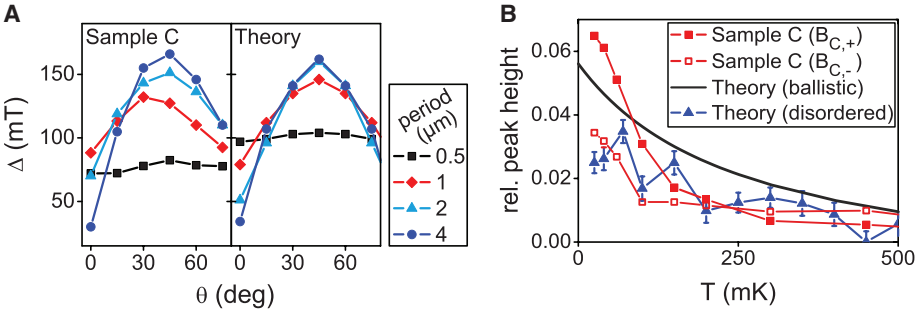

Fig. 4. (**A**) Measured and calculated anisotropy of the stray field, as reflected by the resistance peak separation $\Delta = B_{C,+} - B_{C,-}$. (**B**) Relative resistance peak height $\Delta\rho_{xx}/\rho_{xx}$ as a function of temperature in sample C (solid and open squares for $B_{C,+}$ and $B_{C,-}$, respectively), in the ballistic theoretical model (solid line), and in a model that includes disorder (triangles). In the latter case, the mean free path is 4 μm, and the device length is 18 μm. The stray-field modulation period is 1 μm. The corresponding reference values of the spin-compensated limit are estimated from the resistances at 1 K. Error bars denote the uncertainty in the disorder-averaged values.

References and Notes

1. D. D. Awschalom, D. Loss, N. Samarth, Eds., *Semiconductor Spintronics and Quantum Computation* (Springer, Berlin, 2009).
2. I. Žutić, J. Fabian, S. Das Sarma, *Rev. Mod. Phys.* **76**, 323 (2004).
3. S. Datta, B. Das, *Appl. Phys. Lett.* **56**, 665 (1990).
4. H. C. Koo *et al.*, *Science* **325**, 1515 (2009).
5. J. Schliemann, J. C. Egues, D. Loss, *Phys. Rev. Lett.* **90**, 146801 (2003).
6. B. A. Bernevig, J. Orenstein, S.-C. Zhang, *Phys. Rev. Lett.* **97**, 236601 (2006).
7. J. D. Koralek *et al.*, *Nature* **458**, 610 (2009).
8. J. Fabian, I. Žutić, S. Das Sarma, *Appl. Phys. Lett.* **84**, 85 (2004).
9. N. Rangaraju, J. A. Peters, B. W. Wessels, *Phys. Rev. Lett.* **105**, 117202 (2010).
10. M. Born, V. Fock, *Z. Phys. A* **51**, 165 (1928).

11. L. Landau, *Phys. Sov. Union* **2**, 46 (1932).
12. C. Zener, *Proc. R. Soc. London Ser. A* **137**, 696 (1932).
13. J. K. Furdyna, *J. Appl. Phys.* **64**, R29 (1988).
14. M. König *et al.*, *Phys. Rev. Lett.* **96**, 076804 (2006).
15. T. Koga, Y. Sekine, J. Nitta, *Phys. Rev. B* **74**, 041302(R) (2006).
16. M. V. Berry, *Proc. R. Soc. London Ser. A* **392**, 45 (1984).
17. B. A. Piot *et al.*, *Phys. Rev. B* **82**, 081307 (2010).
18. Materials and methods are available as supplementary materials on *Science* Online.
19. F. J. Teran *et al.*, *Phys. Rev. Lett.* **88**, 186803 (2002).
20. M. Cardona, N. E. Christensen, G. Fasol, *Phys. Rev. B* **38**, 1806 (1988).
21. P. H. Beton *et al.*, *Phys. Rev. B* **42**, 9689 (1990).
22. C. Jia, J. Berakdar, *Phys. Rev. B* **81**, 052406 (2010).
23. M. Calvo, *Phys. Rev. B* **18**, 5073 (1978).
24. O. Zaitsev, D. Frustaglia, K. Richter, *Phys. Rev. B* **72**, 155325 (2005).
25. M. Popp, D. Frustaglia, K. Richter, *Phys. Rev. B* **68**, 041303(R) (2003).
26. J. P. Davis, P. Pechukas, *J. Chem. Phys.* **64**, 3129 (1976).
27. H. Ohno *et al.*, *Nature* **408**, 944 (2000).

Acknowledgments: We thank M. Wimmer for useful discussions and providing the code for the transport equation solver; M. Kiessling for SQUID measurements; M. Wiater for technical assistance in molecular beam epitaxy growth; and C. Back, G. E. W. Bauer, J. Fabian, V. I. Falko, C. Strunk, and G. Woltersdorf for fruitful discussions. We acknowledge financial support from the Deutsche Forschungsgemeinschaft through SFB 689, WE 247618, FOR 1483, and Elitennetzwerk Bayern. Our research in Poland (V.K., G.K., T.W.) was partially supported by the European Union within the European Regional Development Fund, through Innovative Economy grant POIG.01.01.02-00-008/08.

Supplementary Materials

www.sciencemag.org/cgi/content/full/337/6092/324/DC1
Materials and Methods
Supplementary Text
Figs. S1 to S8
Table S1
References (*28*–*39*)

1 March 2012; accepted 14 June 2012
10.1126/science.1221350

A Paramagnetic Bonding Mechanism for Diatomics in Strong Magnetic Fields

Kai K. Lange,[1] E. I. Tellgren,[1] M. R. Hoffmann,[1,2] T. Helgaker[1]*

Elementary chemistry distinguishes two kinds of strong bonds between atoms in molecules: the covalent bond, where bonding arises from valence electron pairs shared between neighboring atoms, and the ionic bond, where transfer of electrons from one atom to another leads to Coulombic attraction between the resulting ions. We present a third, distinct bonding mechanism: perpendicular paramagnetic bonding, generated by the stabilization of antibonding orbitals in their perpendicular orientation relative to an external magnetic field. In strong fields such as those present in the atmospheres of white dwarfs (on the order of 10^5 teslas) and other stellar objects, our calculations suggest that this mechanism underlies the strong bonding of H_2 in the $^3\Sigma_u^+(1\sigma_g 1\sigma_u^*)$ triplet state and of He_2 in the $^1\Sigma_g^+(1\sigma_g^2 1\sigma_u^{*2})$ singlet state, as well as their preferred perpendicular orientation in the external field.

Chemical bonding mechanisms are not only well understood phenomenologically and theoretically, but are also accurately described by the methods of modern quantum chemistry. Molecular atomization energies, for example, are today routinely calculated to an accuracy of a few kilojoules per mole—the "chemical accuracy" characteristic of modern measurements (*1*). However, nearly all our knowledge about chemical bonding pertains to Earth-like conditions, where magnetic interactions are weak relative to the Coulomb interactions responsible for bonding. By contrast, in the atmospheres of rapidly rotating compact stellar objects, magnetic fields are orders of magnitude stronger than those that can be generated in laboratories. In particular, some white dwarfs have fields as strong as 10^5 T, and fields up to 10^{10} T exist on neutron stars and magnetars. Under these conditions, magnetism strongly affects the chemistry and physics of molecules, playing a role as important as that of Coulomb interactions (*2*). To understand this unfamiliar chemistry, we cannot be guided solely by the behavior of molecules under Earth-like conditions. In the absence of direct measurements and observations, ab initio (as opposed to semiempirical) quantum mechanical simulations play a crucial role in unraveling the behavior of molecules in strong magnetic fields and may be useful in the interpretation of white dwarf spectra (*3*, *4*).

Over the years, many quantum chemical studies have been performed on one- and two-electron molecules in strong magnetic fields (*5*). Some of these demonstrate how certain otherwise unbound one-electron molecules become bound in strong fields. Intriguingly, Hartree-Fock calculations by Žaucer and Ažman in 1978 (*6*) and by Kubo in 2007 (*7*) suggest that the otherwise dissociative lowest triplet state $^3\Sigma_u^+(1\sigma_g 1\sigma_u^*)$ of H_2 becomes bound in the perpendicular orientation of the molecule relative to the field. The binding has also been noted in simple model calculations and rationalized in terms of van der Waals binding (dispersion) (*8*) and a shift of electronic charge density toward the molecular center (*9*). Bearing in mind that the uncorrelated Hartree-Fock model often strongly overestimates the binding energy in the absence of magnetic fields, these findings must be confirmed by more advanced quantum chemical simulations.

Here, we report highly accurate calculations on H_2 in strong magnetic fields, taking advantage of our recently developed LONDON code, which is capable of treating molecular systems accurately in all field orientations. Our studies not only confirm the bonding of triplet H_2 but also provide an elementary molecular orbital (MO) explanation that involves neither charge displacement nor dispersion: Nonbonding molecular electronic states are stabilized by the reduction of the paramagnetic kinetic energy of antibonding MOs when these are oriented perpendicular to the magnetic field. The generality of the proposed bonding mechanism is confirmed by calculations on He_2, previously not studied in strong magnetic fields.

To represent the molecular electronic states in magnetic fields, we use the full configuration-interaction (FCI) method [implemented using string-based techniques (*10*–*12*)], where the N-electron wave function is expanded linearly in Slater determinants,

$$|\mathrm{FCI}\rangle = \sum_n C_n \det|\phi_{p_{1n}}, \phi_{p_{2n}}, \ldots \phi_{p_{Nn}}| \qquad (1)$$

whose coefficients C_n are determined by the Rayleigh-Ritz variation principle (*13*). Each determinant is an antisymmetrized product of N orthonormal spin MOs ϕ_p; the summation is over all determinants that may be generated from a given set of MOs. The exact solution to the Schrödinger equation is reached in the limit of a complete set of MOs, making it possible to approach this solution in a systematic manner.

The FCI model makes no assumptions about the structure of the electronic system; in particular, it makes no assumptions regarding the dominance of one Slater determinant (assumed in Hartree-Fock and coupled-cluster theories). This model is therefore capable of describing all bonding situations and dissociation processes in an unbiased manner, which is essential when unfamiliar phenomena are studied. Equally important, the FCI model provides a uniform description of different electronic states and is therefore able to describe the complicated evolution of such states that occurs with increasing field strength.

The FCI method is a standard technique of quantum chemistry, often used to benchmark less expensive and less accurate methods, and was previously used by Schmelcher and Cederbaum in their study of H_2 in strong parallel magnetic fields (*14*). Our FCI implementation differs from

[1]Centre for Theoretical and Computational Chemistry, Department of Chemistry, University of Oslo, N-0315 Oslo, Norway. [2]Chemistry Department, University of North Dakota, Grand Forks, ND 58202, USA.

*To whom correspondence should be addressed. E-mail: trygve.helgaker@kjemi.uio.no